

See discussions, stats, and author profiles for this publication at: <https://www.researchgate.net/publication/231674524>

Structure Determination of Helical Fibers by Numerical Simulation for Small-Angle Neutron Scattering†

ARTICLE *in* LANGMUIR · JULY 2002

Impact Factor: 4.46 · DOI: 10.1021/la025528r

CITATIONS

6

READS

25

3 AUTHORS, INCLUDING:



Hiroshi Fukuda

Kitasato University

63 PUBLICATIONS **433** CITATIONS

SEE PROFILE



Ayako Goto

IUPAC, and Citizen Science Initiative Japan...

45 PUBLICATIONS **614** CITATIONS

SEE PROFILE

Structure Determination of Helical Fiber
by Numerical Simulation for Small-Angle Neutron Scattering

Hiroshi Fukuda ^{1)*}, Ayako Goto ¹⁾, and Toyoko Imae ^{2)*}

¹⁾School of Administration and Informatics, University of Shizuoka, Yada 52-1, Shizuoka 422-8526 and

²⁾Research Center for Materials Science, Nagoya University, Nagoya 464-8602, Japan

Keywords: helical fiber, computer simulation, small-angle neutron scattering, double-strand helix,
single-strand helix, N-octadecanoyl-L-aspartic acid, twisted ribbon.

Running title: Numerical Simulation for SANS of Helical Fiber

Correspondence address: Toyoko Imae

Research Center for Materials Science

Nagoya University

Chikusa, Nagoya 464-8602, Japan

TEL: +81-52-789-5911

FAX: +81-52-789-5912

e-mail: imae@nano.chem.nagoya-u.ac.jp

ABSTRACT: Theoretical equations for the small-angle scattering of double-strand helices with funlike and round cross-sections, as well as a cylinder, were applied to determine the geometry of the self-assembled helical structure formed by N-octadecanoyl-L-aspartic acid ($C_{18}\text{Asp}$). However, those already-known equations were not sufficient to reproduce the experimental small-angle neutron scattering (SANS) curves. Then, a theoretical equation to the small-angle scattering for a helical fiber was derived. The equation with five-fold integration covers the available equations for fibers with finite cross-sections, but it is generalized so as to suit the multi-strand helical structures with arbitrary cross-sectional shapes. Computer simulations based on this theory showed that the best fit to the observed SANS data of $C_{18}\text{Asp}$ fiber is obtained for a model of a single-strand helix with rectangular cross-section, that is, the twisted ribbon.

I. INTRODUCTION

One of commercialized applications of amphiphiles is the utilization as gelators in organic and aqueous mediums. In many cases, fibrous assemblies are formed in gels, forming networks. The morphologies of fibers, which were determined by optical microscopy, transmission electron microscopy (TEM), and atomic force microscopy, are spiral, superhelix, cylinder, hollow tube, double tube, ribbon, platelet, cigar, and ring.¹⁻¹⁶ However, the thickness, length, flexibility, and cross-sectional structure are different from fibers to fibers.

The quantitative analyses of local fiber structures, such as cross-sectional shape and size, were carried out by means of small-angle X-ray scattering (SAXS) and small-angle neutron scattering (SANS). Terech and collaborators¹⁷, using a cylinder model under the consideration of a size distribution, analyzed the scattering data of organogels of steroid surfactants. They found that the thickness of long and rigid rods is slightly sensitive to the solvent species. They¹⁸ carried out the analysis of organogels of 12-hydroxyoctadecanoic acid and its Li salt and found that the aggregates in xylene, hexadecane, decalin, benzene, and fluorobenzene can be described as relatively monodisperse infinitely-long rigid-rods with square cross-section. However, the cross-sectional structure parameters obtained from SANS for fibers in other solvents correspond to elongated rectangular or even lamellar-like (ribbon-like) shape.

Imae et al.¹³ analyzed SANS data of supramolecular fibrils formed in liquid crystals of the ternary system, azo dye/water/methanol. Since the cross-sectional radius obtained from a long rod particle model corresponds to the molecular length, a possible model of fibrils is an arrangement like rodlike micelles. An alternative model is a linear assembly of paired dyes in the antiparallel way. Small-angle

scattering data of hydrogels of fluorinated α -hydrogenated glucophospholipid (F-Glu) were analyzed on the basis of a theoretical equation derived for very long hollow tubules. The wall of tubules appears to consist of three bilayers of F-Glu.¹²

Imae et al.⁷ also reported the formation of fibrous assemblies in 1 % hydrogels of N-acyl-L-aspartic acid (CnASP, n=12,14,16,18) at around neutral pH and at low temperature, although the absolute pH and temperature regions depend on the alkyl chain length. The infinitely long fibrous images were visualized by TEM. The fibers have uniform diameters of 120 Å in minimum and 200 Å in maximum. Minimum and maximum are repeated with a cycle of 650 Å along a contour length, and the fibers seem to take a helical conformation. The cross-sectional radii 22-30 Å for a rod particle model were obtained from the analysis of SANS data for CnAsp fibers. To interpret the data three plausible models were introduced: (a) a double-strand of helical bilayer strands, (b) a superhelical structure of a helical bilayer strand, and (c) a twisted ribbon of a planar bilayer sheet. However, all these models were presented without any theoretical support.

In the present work, we report the structural analysis of fibrous assemblies of C₁₈Asp. In order to determine the most likely structure, theoretical SANS curves were evaluated for different models and compared with the observed data. First, defined structures, such as cylinder and single and double helices, for which the theoretical equations are available, are applied. Then, as an extension of the given above model (c), which was originally proposed for CnAsp fibers,⁷ the theoretical small-angle scattering equation with arbitrary shape of the cross-section is derived. A numerical calculation program in C++ language is introduced to resolve the five-fold integral operation, which is universal for multi-strand helical fibers. From the comparison of the calculated SANS curve with the observed one it

is deduced that the model (c) is the most plausible one for CnAsp fibers.

II. AVAILABLE ANALYTICAL EQUATIONS FOR SMALL-ANGLE SCATTERING OF INFINITELY LONG FIBERS WITH DEFINED CROSS-SECTIONS

(1) Cylinder with round cross -section

It is apparent from TEM photographs that assemblies of CnAsp in gels take a structure of fiber with uniform thickness.⁷ Then, the simplest model of CnAsp fibers is a cylinder. For an infinitely long cylinder with round cross-section of radius R , the small-angle scattering intensity $I(Q)$ at a momentum transfer Q is written by^{19,20}

$$QI(Q) = \left(\frac{2J_1(RQ)}{RQ} \right)^2 \quad (2-1)$$

where $J_1(RQ)$ is a Bessel function. The curve calculated by using Eq. (2-1) is given in Fig. 1(a) and compared with the observed data for C₁₈Asp.⁷ The better fit curve was obtained for $R = 60$ Å, but it is obvious that the observed curve is not reproduced by the cylinder model. The reason for that is the omission of the possible helical conformation of the CnAsp fibers.

(2) Double-strand helix with funlike cross -section

Pringle and Schmidt²¹ derived the equation for the small -angle scattering intensity of helical macromolecules made up of two identical coaxial helixes. The theoretical calculations based on their theory were applied to SAXS of DNA²¹ and SANS of steroidal gels.²⁰ On a model of funlike cross-section, as it can be seen in Fig. 2(a), available equations for an infinitely long helix are as below:

$$QI(Q) = \sum_{n=0}^{\infty} \mathbf{e}_n \cos^2(n\mathbf{j}/2) \frac{\sin^2(n\mathbf{w}/2)}{(n\mathbf{w}/2)^2} [g_n(QR, a)]^2 \quad (2-2)$$

$$g_n(QR, a) = 2R^{-2} (1 - a^2)^{-1} \int_{aR}^R r' J_n(Qr' \sqrt{1 - q_n^2}) dr' \quad (2-3)$$

where

$$q_n = nb / QR \quad \text{at } QR \geq nb$$

$$q_n = 1 \quad \text{at } QR \leq nb$$

$$b = 2\mathbf{p}R / P$$

$$\mathbf{e}_0 = 1 \quad \text{and} \quad \mathbf{e}_n = 2 \quad \text{at } n \geq 1 \quad (2-4)$$

The parameters \mathbf{j} , \mathbf{w} , R , and a are defined in Fig. 2(a). P is the helical pitch. If $\mathbf{j} = \mathbf{p}$, the center angle of fun is given by Eq. (2-5).

$$\mathbf{w} = 2 \sin^{-1} \frac{r}{R} \quad (2-5)$$

Figure 1(b) shows the curve which was calculated with the optimum parameters: $R = 100\text{\AA}$, $r = 30\text{\AA}$, $\theta = 35^\circ$, and $P = 1300 (= 650 \times 2)\text{\AA}$ when $a = 0$ and $\mathbf{j} = \mathbf{p}$. It can be clearly seen that the calculated curve, in the Q region above 0.03\AA^{-1} , does not fit to the observed data.

(3) Single- and Double-strand helixes with round cross-section

An alternative theoretical equation for the small-angle scattering intensity of a double-strand helix was reported by Puigjaner and Subirana.²² The double-strand helix with round cross-section is situated as shown in Fig. 2(b), where the fiber axis is equivalent to a z axis. In this figure, r_1 and r_2 are the cross-sectional radii of the two cylinders, \mathbf{d}_1 and \mathbf{d}_2 are the distances from the fiber axis to the centers of the cross-sections, and \mathbf{a} is the angle between the two cylinders. Then the scattering intensity is described by Eq. (2-6).

$$QI(Q) = \sum_n (a_{1n}^2 + a_{2n}^2 + 2a_{1n}a_{2n} \cos n\mathbf{a}) \quad (2-6)$$

where

$$a_{in} = J_1(\mathbf{d}_i Q_\perp) \mathbf{p}_i^2 \frac{2J_1(r_i Q_\perp)}{r_i Q_\perp}$$

$$Q_\perp^2 = Q^2 - \left[\frac{2\mathbf{p}}{P} \right]^2 \quad (2-7)$$

P is the helical pitch, and Q_\perp is the component of Q in the x - y plane. It is noted that these equations, for $\mathbf{a} = 0$, correspond to the small-angle scattering intensity of a single-strand helix.

The curve for a double-strand helix with the optimum parameters $r_1 = r_2 = r = 30$ Å, $\mathbf{d}_1 = \mathbf{d}_2 = \mathbf{d} = 70$ Å, $\mathbf{a} = \mathbf{p}$, and $P = 1300$ Å is drawn in Fig. 1(c), and the curve for a single-strand helix with the optimum parameters $r_1 = r_2 = r = 30$ Å, $\mathbf{d}_1 = \mathbf{d}_2 = \mathbf{d} = 70$ Å, $\mathbf{a} = 0$, and $P = 1300$ Å is drawn in Fig. 1(d). Non-agreement to the observed data is observed, especially, in the lower Q region. This indicates that even helix models with round cross-section are not enough to interpret the structure of CnAsp fibers.

III. NUMERICAL COMPUTATION FOR SMALL-ANGLE SCATTERING OF INFINITELY-LONG HELICAL FIBERS WITH ARBITRARY CROSS-SECTIONS

The single- and double-strand helices with round cross-section above mentioned are just the models (b) and (a), respectively, which are two of the three plausible models introduced to explain the structure of CnAsp fibers. Since both helical models were found to be inadequate, the other model (c) has been examined. However, since theoretical equations for the model (c) are not available, the corresponding equation must be first derived. We introduce here the universal equation for the

small-angle scattering of multi-strand helix with arbitrary cross-sections.

For deriving a general equation of the scattering intensity from helical fibers, the geometry of the cross-section in the x-y plane is defined as it is shown in Fig. 3. The coordinate (x_0, y_0) of an origin of the cross-section of a fiber is located at distance d from the main axis z of the helical fiber. Since the cross-section with an arbitrary shape rotates at a pitch P around the helix axis, a matrix $R(\mathbf{q})$, as it is given in Eq. (3-1), is used for the transfer of the rotational angle \mathbf{q} in the x-y coordinate.

$$R(\mathbf{q}) = \begin{pmatrix} \cos \mathbf{q} & -\sin \mathbf{q} \\ \sin \mathbf{q} & \cos \mathbf{q} \end{pmatrix} \quad (3-1)$$

where

$$\mathbf{q} = 2\pi \mathbf{r} / P \quad (3-2)$$

The scattering intensity $I_1(\mathbf{Q})$ of a fiber is described by a Fourier transform of the scattering length density $\mathbf{r}(\mathbf{r})$ in the real space. Then,

$$I_1(\mathbf{Q}) = |A(\mathbf{Q})|^2 \quad (3-3)$$

$$A(\mathbf{Q}) = \int d\mathbf{r} \mathbf{r}(\mathbf{r}) e^{i\mathbf{Q}\mathbf{r}} \quad (3-4)$$

where a momentum transfer vector \mathbf{Q} and a position vector \mathbf{r} , respectively, are written by

$$\mathbf{Q} = (Q_x, Q_y, Q_z) = (\mathbf{Q}_\perp, Q_z) \quad (3-5)$$

$$\mathbf{r} = (x, y, z) = (\mathbf{r}_\perp, z) \quad (3-6)$$

When the position vector of an origin of the cross-section is \mathbf{r}_0 ,

$$\mathbf{r}_0 = (x_0, y_0, z_0) = (\mathbf{r}_{0\perp}, z_0) \quad (3-7)$$

the scattering length density for a fiber of length L is divided into two terms and described by

$$\mathbf{r}(\mathbf{r}) = \mathbf{r}_\perp (R(-\mathbf{q})\mathbf{r}_\perp - \mathbf{r}_{0\perp}) \Pi(z, L) \quad (3-8)$$

where $\mathbf{r}_\perp(x, y)$ is the scattering length density from the origin (x_0, y_0) on the x-y plane and

$$\Pi(z, L) = 1 \quad \text{for} \quad |z| \leq L/2$$

$$= 0 \quad \text{for otherwise} \quad (3-10)$$

When substituting Eq. (3-8) into Eq. (3-4) and replacing the integral variable \mathbf{r}_\perp to $R(-\mathbf{q})\mathbf{r}_\perp - \mathbf{r}_{0\perp}$, we obtain

$$A(\mathbf{Q}) = \int d\mathbf{r}_\perp \mathbf{r}_\perp(\mathbf{r}_\perp) e^{iR(\mathbf{q})\mathbf{Q}_\perp \cdot (\mathbf{r}_\perp + \mathbf{r}_{0\perp})} \int dz \Pi(z, L) e^{iQ_z z} \quad (3-11)$$

The scattering intensity $I_{en}(Q)$ for an ensemble of randomly dispersed fibers in a system is obtained by space-averaging the scattering intensity of a fiber $I_1(\mathbf{Q})$, according to the geometry illustrated in

Fig. 4, where

$$\mathbf{Q}_\perp = \begin{pmatrix} Q \sin \Theta \cos \Phi \\ Q \sin \Theta \sin \Phi \end{pmatrix} \quad (3-12)$$

$$Q_z = Q \cos \Theta \quad (3-13)$$

The resulting scattering intensity is

$$\begin{aligned} I_{en}(Q) &= \frac{1}{4\mathbf{p}} \int_0^{2\mathbf{p}} d\Phi \int_0^{\mathbf{p}} \sin \Theta d\Theta |I_1(\mathbf{Q})|^2 \\ &= \frac{1}{4\mathbf{p}} \int_0^{2\mathbf{p}} d\Phi \int_0^{\mathbf{p}} \sin \Theta d\Theta \left| \int \mathbf{r}_\perp(\mathbf{r}_\perp) e^{iR(\mathbf{q})\mathbf{Q}_\perp \cdot (\mathbf{r}_\perp + \mathbf{r}_{0\perp})} d\mathbf{r}_\perp \int_{-L/2}^{L/2} e^{iQ_z z} dz \right|^2 \end{aligned} \quad (3-14)$$

We rewrite the scattering intensity (3-14) to a more convenient form for numerical calculation making the range of the z integral independent of the length L of the fiber. Since $R(\mathbf{q})$ is a periodic function of a period $2\mathbf{p}$, if we describe the length of a fiber by

$$L = mP \quad m: \text{odd integer} \quad (3-15)$$

we obtain the following expression for the scattering intensity.

$$I(Q; m) = \frac{1}{4\mathbf{p}mP} \int_0^{2\mathbf{p}} d\Phi \int_0^{\mathbf{p}} \sin \Theta d\Theta \left| c_m(PQ_z) \int \mathbf{r}_\perp(x, y) e^{iR(\mathbf{q})\mathbf{Q}_\perp \cdot (\mathbf{r}_\perp + \mathbf{r}_{0\perp})} dx dy \int_{-P/2}^{P/2} e^{iQ_z z} dz \right|^2 \quad (3-16)$$

where

$$c_m(PQ_z) = 1 + 2 \cos PQ_z + \dots + 2 \cos \frac{m+1}{2} PQ_z \quad (3-17)$$

Hence, for infinitely long fibers we obtain

$$I_{\text{inf}}(Q) = \lim_{m \rightarrow \infty} I(Q; m) \quad (3-18)$$

For the scattering intensity of multi-strand helical fibers, $\mathbf{r}_{\perp}(x, y)$ is described as a sum of the cross-section components of the fiber. The shape of the cross-section is alterable by the integrand of x and y , that is, $\mathbf{r}_{\perp}(x, y)$.

The five-fold integrals of Φ , Θ , x , y , and z in the finite range given by Eq. (3-16) can be calculated according to the Gauss-Legendre method.²³ For a numerical calculation, it is convenient to define $\mathbf{r}_{\perp}(x, y)$ of the helix by the inheritance of the class in C++ language. We defined the following 'section_list' class in C++ language and then any $\mathbf{r}_{\perp}(x, y)$ from the origin (x_0, y_0) by the inherited classes of it.

```
class section_list
{
protected:
    static double Q; //momentum transfer
    double QRx0 const; // x component of  $R(\mathbf{q})Q_{\perp}$  in Eq. (3-16)
    double QRy0 const; // y component of  $R(\mathbf{q})Q_{\perp}$  in Eq. (3-16)
    cmplx expxy(double x, double y) const; //  $e^{iQ_{\perp}r_{\perp}}$  in Eq. (3-16)
public:
    double x0, y0; // origin of the cross section from the axis of the helix  $(x_0, y_0)$ 
    void add(); // add the cross section to the helix
    virtual inline cmplx figure() const = 0; // define cross section
};
```

Small-angle scattering curves for double-strand helices calculated using the theoretical equation

derived above were compared with those from available equations (2-2) and (2-6). Model calculations with $m=7$ and the same geometrical parameters of fibers were perfectly consistent with those from latter ones, which were shown in Fig. 1, for helices with funlike and round cross-sections. This indicates that the derived equation is exactly equivalent to the available equations already reported, if we use sufficiently large m . In fact, for $m=7$, the length of helical object $L = 7 \times 1300 \text{ \AA}$ is sufficiently large compared with the cross-sectional radius of object, several tenth \AA .

IV. HELICAL FIBER SELF-ASSEMBLED BY AMINO ACID SURFACTANT

As discussed above, it is doubtful that the single- and double-strands of helical bilayer strands (models (b) and (a)), modeled as single- and double-strand helices with round cross-sections, respectively, are adequate models for CnAsp fibers. Then, the equation (3-16) derived was applied to the model (c) of a twisted ribbon. A twisted ribbon of a planar bilayer sheet (model (c)) can be regarded as a single-strand helix with rectangular cross-section. A computer simulation was then carried out on the basis of this model, and the corresponding small-angle scattering curves, calculated with the optimum parameters, were compared with the observed SANS curve of C₁₈Asp fibers⁷, as it is shown in Fig. 5(a). The fitting to the observed curve is the best for the calculation based on a single-strand helix with rectangular cross-section with the following parameters: long-width $W = 180 \text{ \AA}$, short-width $H = 50 \text{ \AA}$, and helical pitch $P = 1300 \text{ \AA}$. Since the good fitting spans now to regions of up to $Q = 0.2 \text{ \AA}^{-1}$, it is concluded that the helical ribbon is the best model of CnAsp fibers.

The effect of the variation of the parameters was examined, and this can be seen in Figs. 6 ~ 8. As the short-width of rectangular cross-section is shortened from 50 \AA to 40 \AA , the $I(Q)$ vs. Q curve

becomes more gradual and a peak at around $Q = 0.02 \text{ \AA}^{-1}$ shifts to larger Q values (see Fig. 6). This tendency is consistent with that observed in SANS curves for $C_{18}\text{Asp}$ to $C_{14}\text{Asp}$ fibers.⁷ If the rectangular cross-section is formed by bilayers, the short width must be the double of the molecular length. Since the calculated molecular lengths of $C_n\text{Asp}$ ($n = 14, 16, 18$) are 22.5, 25.0, and 27.5 Å, respectively,⁷ the double of their lengths are consistent with the variation of the short width, if the alkyl chains are slightly tilt or melt. Figure 7 shows the effect of the long width in rectangular cross-section. Even if the width is changed from 160 to 200 Å, the calculated intensity curves are scarcely affected. This suggests that the size distribution of long widths is insensitive to the scattering curves. Similar conclusions were obtained for the helical pitch. As it is seen in Fig. 8, the changes of the helical pitch in the range 1100 ~ 1300 Å, which is within the observed error, give a meaningless influence to the scattering curves.

Based upon the numerical simulation, it is then considered that the twisted ribbon model, that is, the single-strand helix with rectangular cross-section is the best fitted model for the $C_n\text{Asp}$ fibers, in which the cross-section of the ribbon consists of a bilayer of the component molecules. However, this twisted ribbon is not reasonable from the viewpoint of a self-assembly structure, because the alkyl chains in the edge of the bilayer are exposed to bulk water. Therefore, another model was proposed, as it is shown in Fig. 5(b). In this case two semicircular assemblies of component molecules are attached on both edges to the ribbon in order to inhibit the direct contact of the alkyl chains with the bulk water. According to this model with edge-covered rectangular cross-section, the fitting curve was drawn and it is shown in Fig. 5(b). Since the fitting curve deviates slightly in the region of small Q , this model does not seem to be the most plausible one considering the self-assembly of the fibers. It was reported that

bilayer ribbon's edges are different from entire ribbon surface in the character and the twisted bilayer ribbons close to yield tubes.²⁴ This supports the rectangular cross-section without covered edges as determined above.

V. CONCLUSIONS

The available theoretical equations so far for small-angle scattering of fibers were separately introduced for different kinds of structures. One inconvenience for utilizing them is the separate programming, when the different structures are compared. Other demerit is that its use is limited to structures where the theoretical equations are available. Theoretical analyses for double-strand helix models were carried out using the available equations. However, such trial did not succeed to reproduce the SANS curves of CnAsp fibers. As the single-strand helix is another possibility for modeling CnAsp fibers, the corresponding theoretical equations were derived in this work.

Since the strict equation for the calculation consists of a five-fold integral equation, the calculation is troublesome. However, if one programs at once the universal equation, this program can be used for the calculation of the small-angle scattering of fibers with any kind of cross-sectional shape. The equation can be used even for a multi-strand helix and also for a helix with inhomogeneous scattering length. From the application of this equation to CnAsp fibers, it was concluded that the fibers must be twisted ribbons. The cross-section of ribbons consists of a bilayer of the component molecules, being the width 3~4 times larger than the bilayer thickness.

Acknowledgement: We thank for Mr. Yingqun Fang and Ms. Hiroko Tanaka for their help in numerical

computation.

References

- 1 (a) T. Tachibana and H. Kambara, *J. Am. Chem. Soc.* 87, 3015 (1965); (b) T. Tachibana, S. Kitagawa, and H. Takeno, *Bull. Chem. Soc. Jpn.* 43, 2418 (1970).
- 2 (a) H. Hidaka, M. Miura, and T. Onai, *J. Chem. Soc., Chem. Commun.* 562 (1984); (b) H. Hidaka *Colloids Surf.* 58, 1 (1991).
- 3 (a) N. Nakashima, S. Asakuma, J.-M. Kim, and T. Kunitake, *Chem. Lett.* 1709 (1984); (b) N. Nakashima, S. Asakuma, and T. Kunitake, *J. Am. Chem. Soc.* 107, 509 (1985).
- 4 (a) R. H. Wade, P. Terech, E. A. Hewat, R. Ramasseul, and F. Volino, *J. Colloid Interface Sci.* 114, 442 (1986); (b) P. Terech and R. H. Wade, *J. Colloid Interface Sci.* 125, 542 (1988).
- 5 (a) J.-H. Fuhrhop, P. Schnieder, J. Rosenberg, and E. Boekema, *J. Am. Chem. Soc.*, 109, 3387 (1987); (b) J.-H. Fuhrhop, S. Svenson, C. Boettcher, E. Rossler, H.-M. Vieth, *J. Am. Chem. Soc.* 112, 4307 (1990).
- 6 H. Yanagawa, Y. Ogawa, H. Furuta, K. Tsuno, *Chem. Lett.* 269 (1988); *Chem. Lett.* 403 (1989); *J. Am. Chem. Soc.* 111, 4567 (1989).
- 7 (a) T. Imae, Y. Takahashi, and H. Muramatsu, *J. Am. Chem. Soc.* 114, 3414 (1992); (b) T. Imae and S. Kidoaki, *J. Jpn. Oil Chem. Soc.* 44, 301 (1995); (c) T. Imae, N. Hayashi, T. Matsumoto, T. Tada, and M. Furusaka, *J. Colloid Interface Sci.* 225, 285 (2000).
- 8 (a) K. Hanabusa, K. Okui, K. Karaki, T. Koyama, and H. Shirai, *J. Chem. Soc., Chem. Commun.* 1371 (1992); (b) K. Hanabusa, Y. Matsumoto, T. Miki, T. Koyama, and H. Shirai, *J. Chem. Soc., Chem.*

Commun. 1401 (1994).

9 T. Gulik-Krzywicki, C. Fouquey, and J. -M. Lehn, Proc. Natl. Acad. Sci. U.S.A. 90, 163 (1993).

10 S. Bonaccio, M. Wessicken, D. Berti, P. Walde, and P. L. Luisi, Langmuir, 12, 4976 (1996).

11 (a) T. Shimizu, M. Kogiso, and M. Masuda, Nature 383, 487 (1996); (b) T. Shimizu and M. Masuda, J. Am. Chem. Soc. 119, 2812 (1997).

12 (a) T. Imae, M. -P. Krafft, F. Giulieri, T. Matsumoto, and T. Tada, Progr. Colloid Polym. Sci., 106, 52 (1997); (b) M. P. Krafft and J. G. Riess, Bi ochimie 80, 489 (1998); (c) T. Imae, K. Funayama, M. -P. Krafft, F. Giulieri, T. Tada, and T. Matsumoto, J. Colloid Interface Sci. 212, 330 -337 (1999).

13 T. Imae, L. Gagel, C. Tunich, G. Platz, T. Iwamoto, and T. Funayama, Langmuir, 14, 2197 (1998).

14 V. Emmanouil, M. El Ghoul, C. André -Barrès, B. Guidetti, I. Rico -Lattes, and A. Lattes, Langmuir, 14, 5389 (1998).

15 (a) T. Imae, Y. Ikeda, M. Iida, N. Koine, and S. Kaizaki, Langmuir 14, 5631 (1998); (b) Y. Ikeda, T. Imae, M. Iida, N. Koine, and S. Kaizaki, Langmuir, 17, 361 (2001).

16 N. Yamada, K. Ariga, M. Naito, K. Matsubara, and E. Koyama, J. Am. Chem. Soc. 120, 12192 (1998).

17 (a) P. Terech, Progr. Colloid Polym. Sci. 82, 263 (1990); (b) T. Terech, I. Furman, and R. G. Weiss, J. Phys. Chem. 99, 9558 (1995).

18 (a) P. Terech, Colloid Polym. Sci. 269, 490 (1991); J. Phys. II France 2, 2181 (1992); (b) P. Terech, V. Rodriguez, J. D. Barnes, and G. B. McKenna, Langmuir, 10, 3406 (1994).

19 B. K. Vainshtein, in Diffraction of X -rays by chain molecules (El sevier, New York, 1966).

20 P. Terech, F. Volino, and R. Ramasseul, J. Physique 46, 895 (1985).

21 O. A. Pringle and P. W. Schmidt, J. Appl. Cryst. 4, 290 (1971).

22 L. C. Puigjaner and J. A. Subirana, *J. Appl. Cryst.* 7, 169 (1974).

23 M. Abramowitz and I. A. Stegun, *Handbook of mathematical functions*, (Dover; 1970).

24 M. Goren, Z. Qi, and B. Lennox, *Chem. Matt.* 12, 1220 (2000).

Figure Captions

Figure 1. Comparison of model calculations using Eqs. (2-1), (2-2), and (2-6) and the observed SANS curve. Solid line: calculated curves for (a) cylinder ($R = 60 \text{ \AA}$); (b) double-strand helix with funlike cross-section ($R = 100 \text{ \AA}$, $r = 30 \text{ \AA}$, $\theta = 35^\circ$, $a = 0$, $\mathbf{j} = \mathbf{0}$, $P = 1,300 \text{ \AA}$); (c) double-strand helix with round cross-section ($r_1 = r_2 = r = 30 \text{ \AA}$, $\theta_1 = \theta_2 = \theta = 70 \text{ \AA}$, $\theta = 0$, $P = 1300 \text{ \AA}$). (d) single-strand helix with round cross-section ($r_1 = r_2 = r = 30 \text{ \AA}$, $\theta_1 = \theta_2 = \theta = 70 \text{ \AA}$, $\theta = 0$, $P = 1300 \text{ \AA}$). Broken line: observed curve for $C_{18}\text{Asp}$ fiber in a 1 wt% aqueous solution. ⁷ Cross-section models were shown.

Figure 2. Geometry of the cross-section of a double-strand helical fiber in the x-y plane of Cartesian coordinates. (a) funlike cross-section; (b) round cross-section.

Figure 3. Geometry of the cross-section of a fiber in the x-y plane of Cartesian coordinates.

Figure 4. Notation of Q in Cartesian coordinates.

Figure 5. Comparison of model calculations using a five-fold integral equation for a twisted ribbon and the observed SANS curve. Solid line: calculated curves for (a) single-strand helix with rectangular cross-section ($W = 180 \text{ \AA}$, $H = 50 \text{ \AA}$, $P = 1300 \text{ \AA}$); (b) single-strand helix with edge-covered rectangular cross-section ($W = 130 \text{ \AA}$, $H = 50 \text{ \AA}$, $P = 1300 \text{ \AA}$). Broken line: observed curve for $C_{18}\text{Asp}$ fiber in a 1 wt% aqueous solution. ⁷ Cross-section models were shown.

Figure 6. Comparison of model calculations using a five -fold integral equation for a twisted ribbon and the observed SANS curve. Solid line: calculated curves as a variation of short-width of rectangular cross-section. Broken line: observed curve for C₁₈Asp fiber in a 1 wt% aqueous solution.⁷ Used parameters are given in the Figure.

Figure 7. Comparison of model calculations using a five -fold integral equation for a twisted ribbon and the observed SANS curve. Solid line: calculated curves as a variation of long-width of rectangular cross-section. Broken line: observed curve for C₁₈Asp fiber in a 1 wt% aqueous solution.⁷ Used parameters are given in the Figure.

Figure 8. Comparison of model calculations using a five -fold integral equation for a twisted ribbon and the observed SANS curve. Solid line: calculated curves as a variation of helical pitch. Broken line: observed curve for C₁₈Asp fiber in a 1 wt% aqueous solution.⁷ Used parameters are given in the Figure.

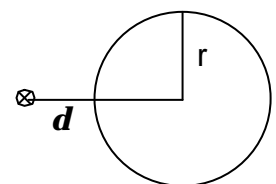
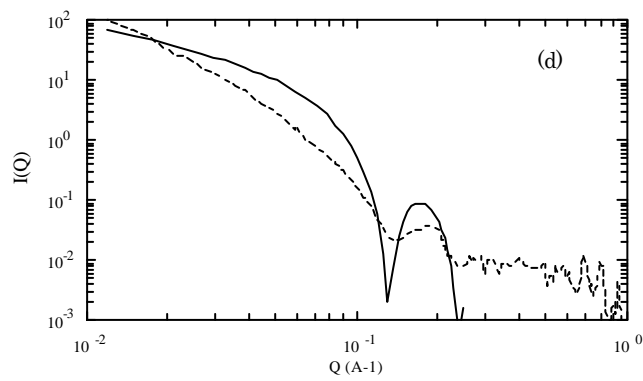
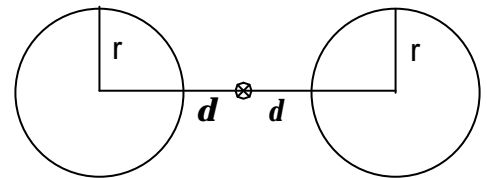
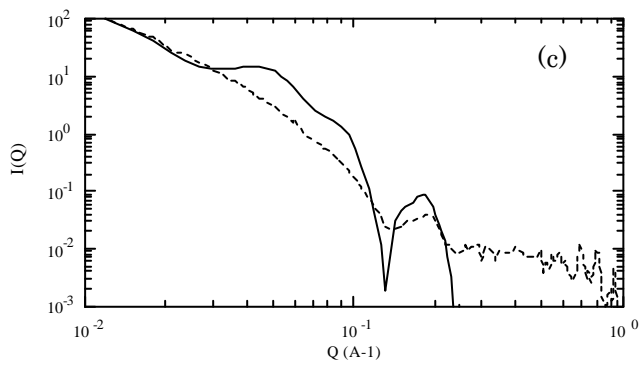
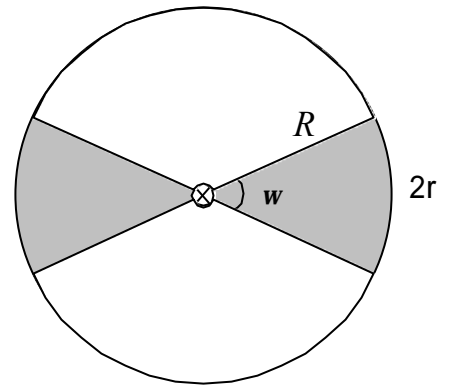
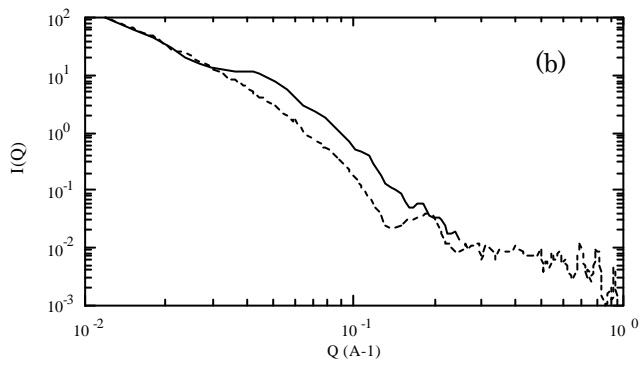
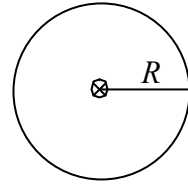
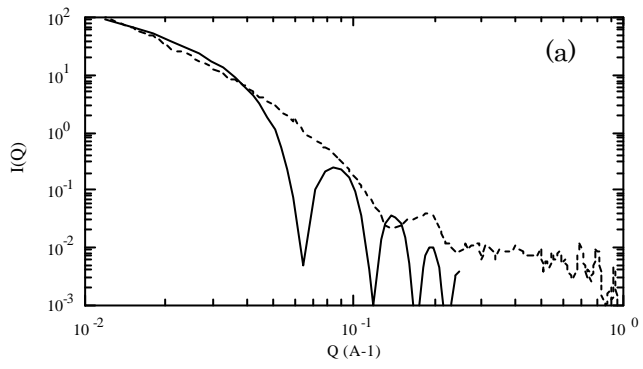


Fig.1 Fukuda et al.

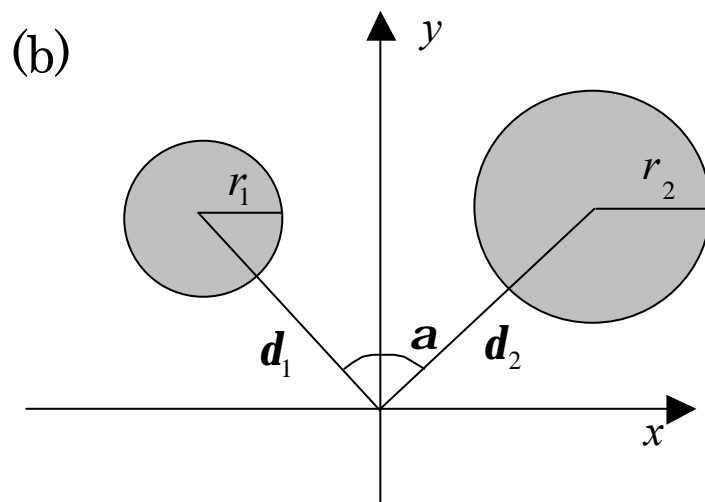
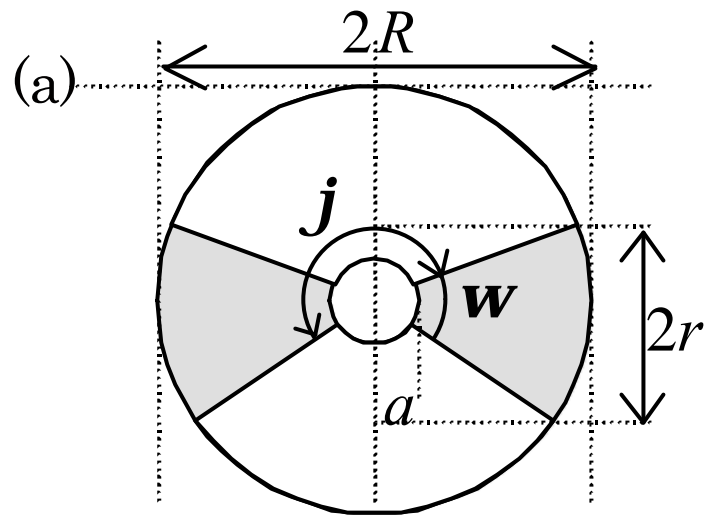


Fig.2 Fukuda et al.

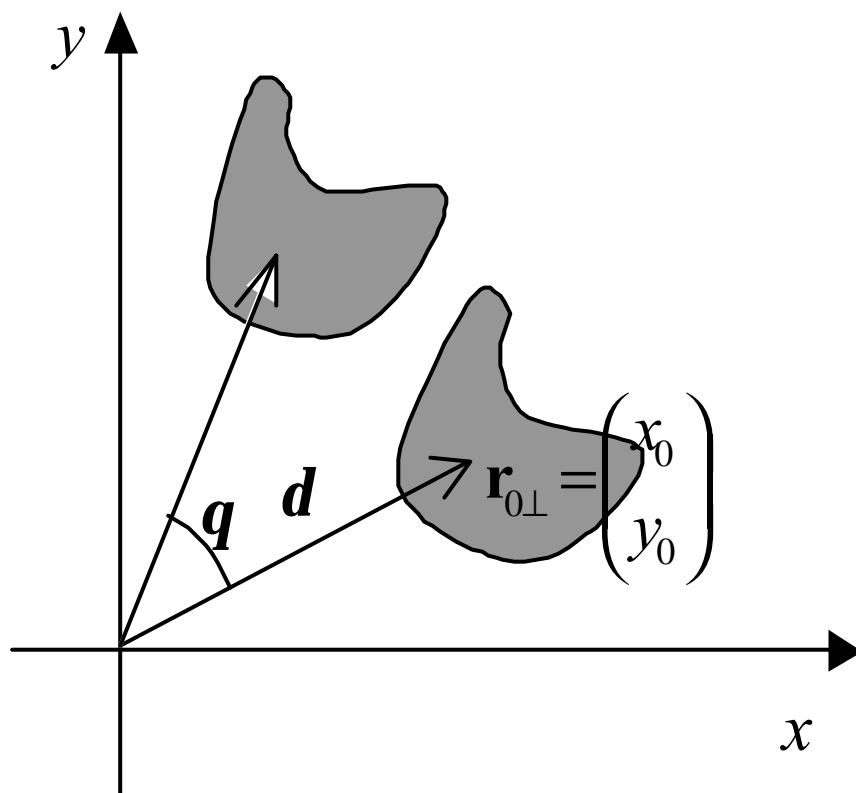


Fig.3 Fukuda et al.

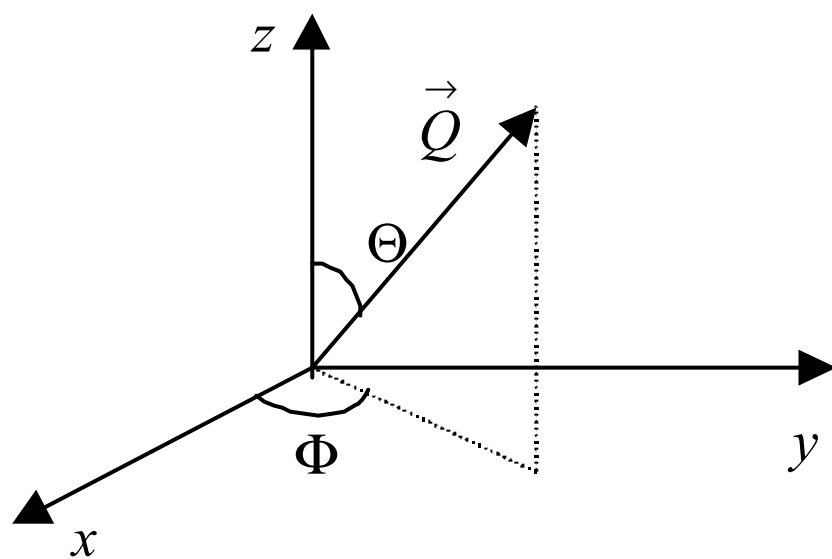
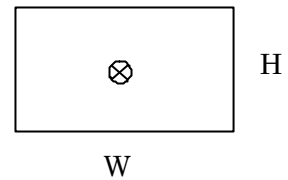
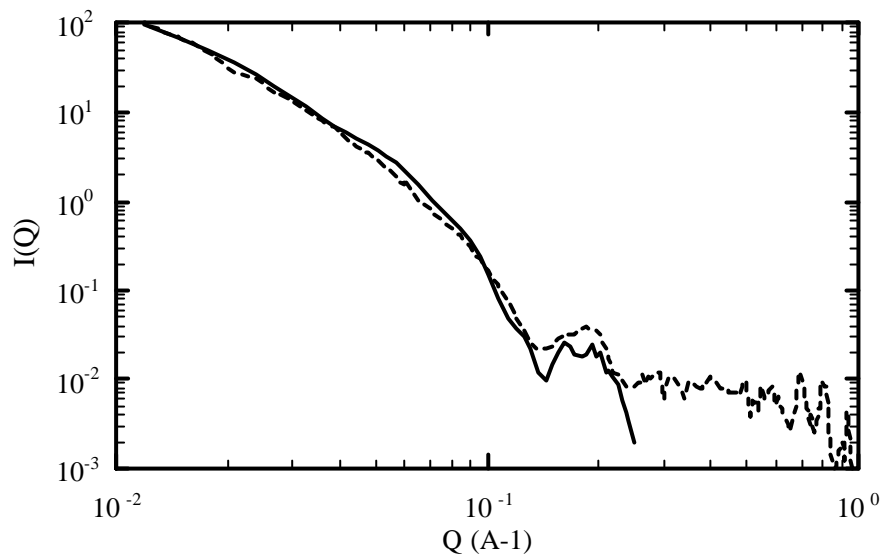


Fig.4 Fukuda et al.

(a) $W = 180 \text{ A}$, $H = 50 \text{ A}$, $P = 1300 \text{ A}$



(b) $W=130 \text{ A}$, $H=50 \text{ A}$, $P=1300 \text{ A}$

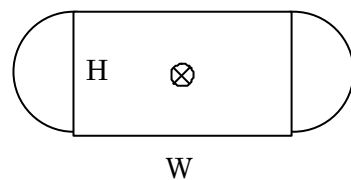
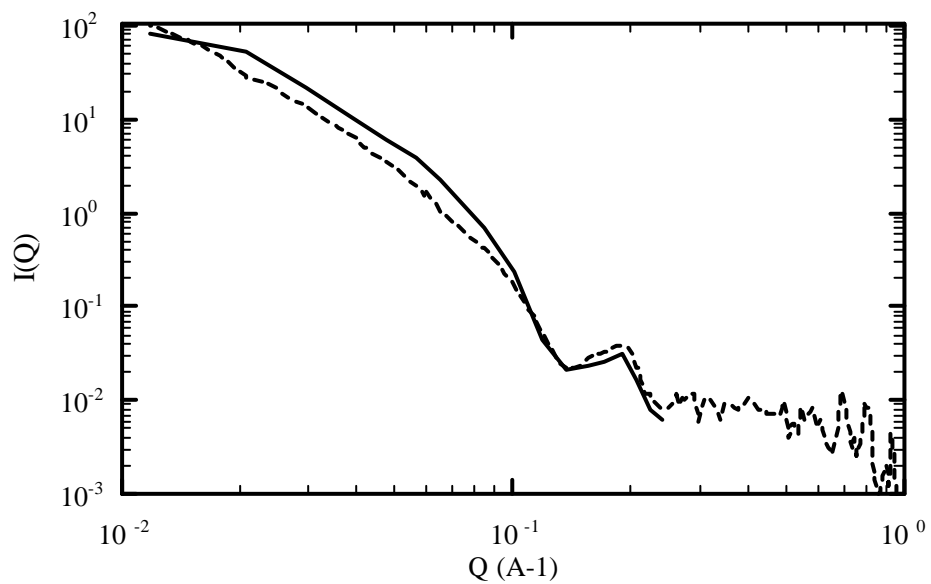
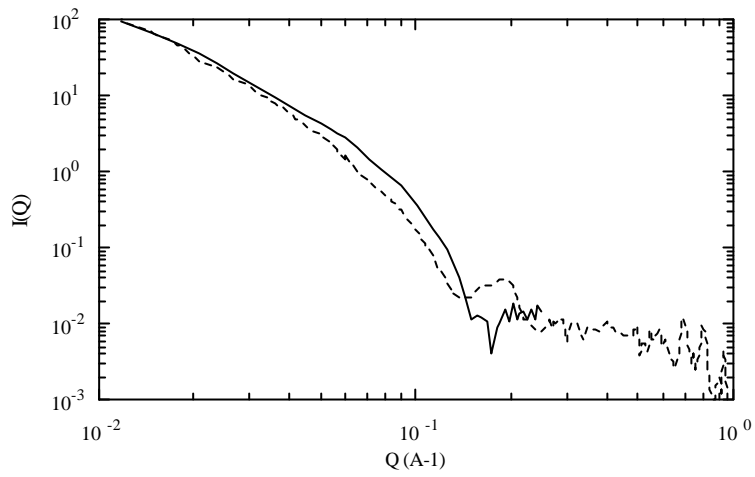
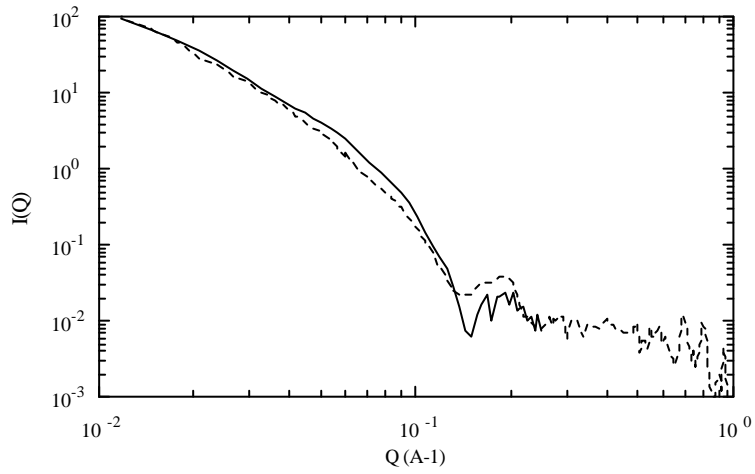


Fig.5 Fukuda et al.

W=180 A, H=40 A, P=1300 A



W=180 A, H=45 A, P=1300 A



W=180 A, H=50 A, P=1300 A

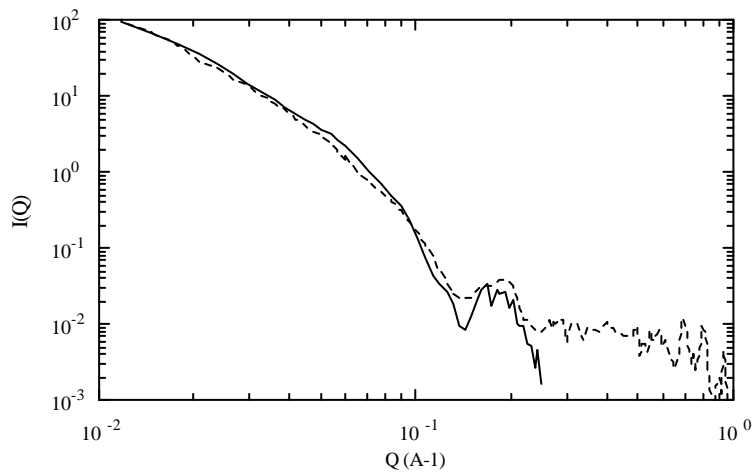
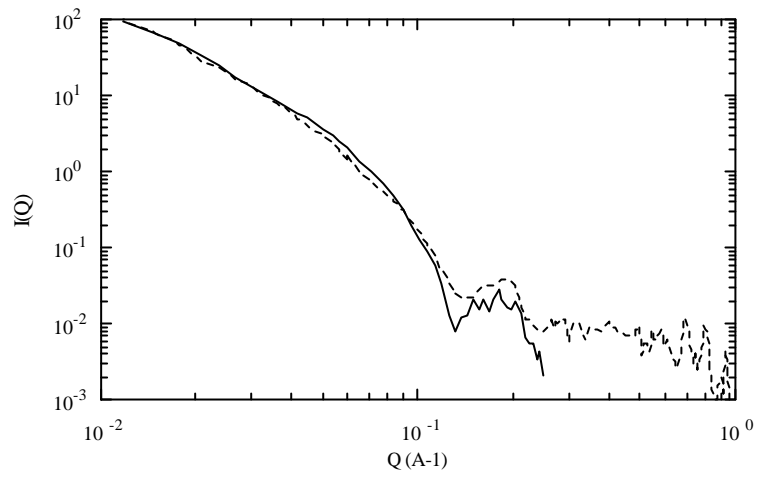
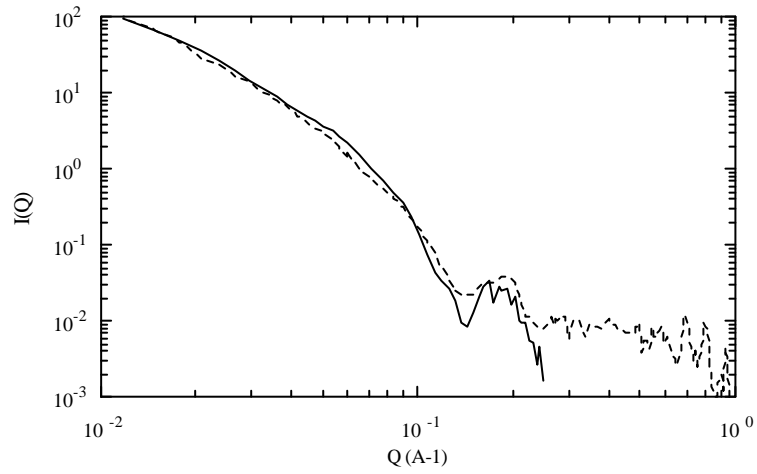


Fig.6 Fukuda et al.

W=200 A, H=50 A, P=1300 A



W=180 A, H=50 A, P=1300 A



W=160 A, H=50 A, P=1300 A

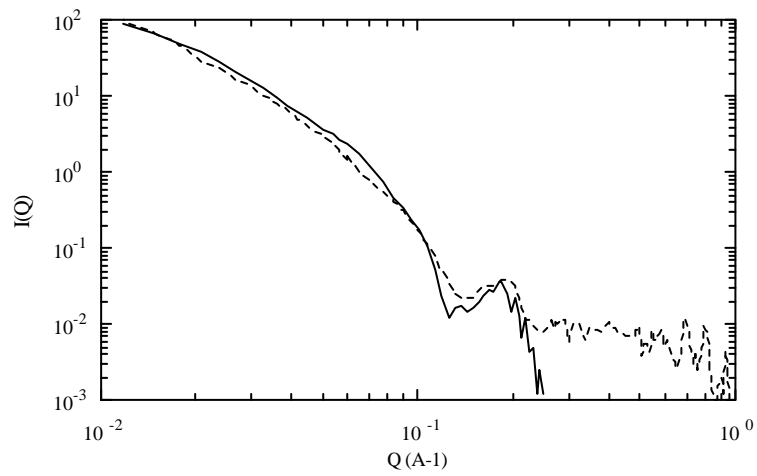
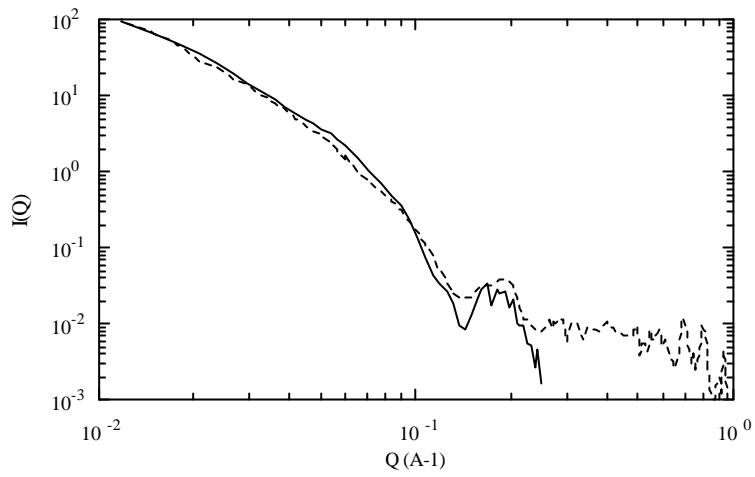
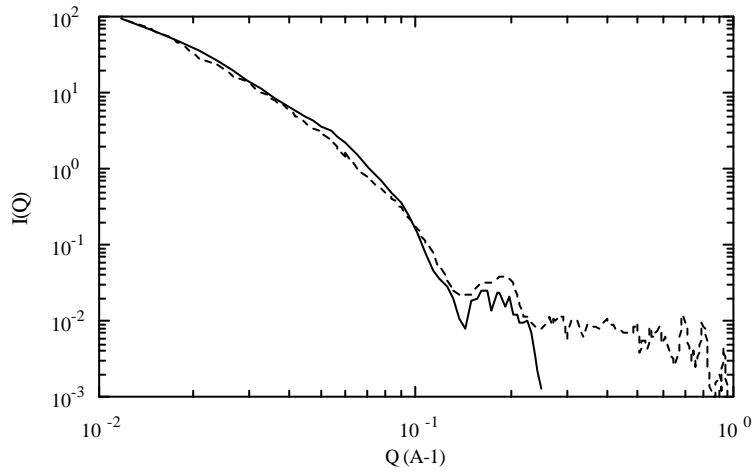


Fig.7 Fukuda et al.

W=180 A, H=50 A, P= 1300 A



W=180 A, H=50 A, P= 1200 A



W=180 A, H=50 A, P= 1100 A

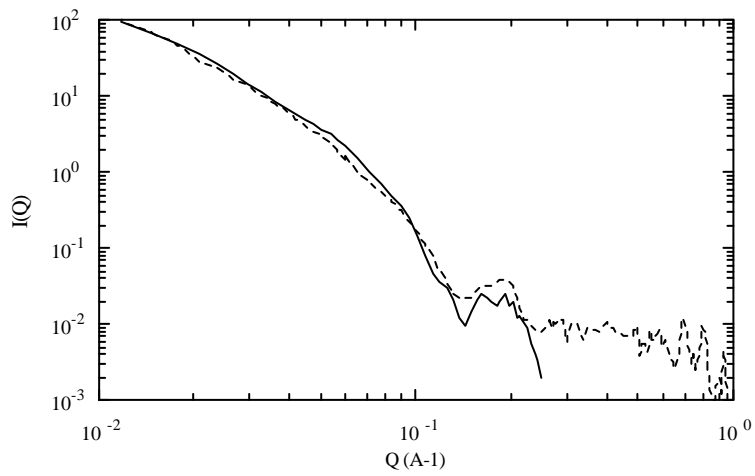


Fig.8 Fukuda et al.